TABLE 1 Summary of Input Impedance of Dipole Antenna

Mesh Types	Cell Size	No. of Cells	Time	Resonant Freq (GHz)	Impedance (Ω)
Fine mesh	$\Delta x = 0.1$ mm $\Delta y = 0.1$ mm $\Delta z = 0.2$ mm	$20 \times 20 \times 501$	0:3:12	1.38	73+j0
Large Δz	$\Delta x = 0.1$ mm $\Delta y = 0.1$ mm $\Delta z = 0.6$ mm	$20 \times 20 \times 168$	0:1:43	1.325	88+j0
Nonuniform	$\Delta x = 0.1$ mm $\Delta y = 0.1$ mm $\Delta z = 0.2$ mm	$20 \times 20 \times 115$	0:1:49	1.38	73+j0
Subgridding (Δzratio = 3:1)	$\Delta x = 0.1$ mm $\Delta y = 0.1$ mm $\Delta z = 0.6$ mm	$20 \times 20 \times 168$	0:6:59	1.375	78+j0
Coarse mesh	$\Delta x = 0.5$ mm $\Delta y = 0.5$ mm $\Delta z = 1.0$ mm	$4 \times 4 \times 101$	0:1:14	1.383	73+j0

ACKNOWLEDGMENTS

This research is partially sponsored by Communication University of China under 111 project.

REFERENCES

1. A. Taflove and S. Hagness, Computational electromagnetics: The finite-difference time-domain method, 3rd ed., Artech House, Norwood, 2005.
2. W. Yu, R. Mittra, T. Su, Y. Liu, and X. Yang, Parallel finite difference time domain method, Artech House, Norwood, 2006.
3. R. Harrington, Time-harmonic electromagnetic fields, IEEE Press, Piscataway, NJ, 2001.
4. J. Jin, The finite element method in electromagnetics, Wiley, New York, 2002.
5. GEMS software package, Computer and communication unlimited, State College, PA.

AN ALTERNATIVE ANALYTICAL REDUCTION SCHEME IN THE TIME-DOMAIN LAYERED FINITE ELEMENT REDUCTION RECOVERY METHOD FOR HIGH-FREQUENCY IC DESIGN

Houle Gan and Dan Jiao
School of Electrical and Computer Engineering, Purdue University, West Lafayette, IN 47907; Corresponding author: djiao@purdue.edu

Received 28 December 2007

ABSTRACT: *An alternative analytical reduction scheme was proposed in the time-domain layered finite element reduction recovery (LAFE-RR) method for the analysis of high-frequency integrated circuits. This alternative reduction scheme permits the use of general absorbing boundary conditions in the framework of a time-domain LAFE-RR method. In addition, it allows for an application of the LAFE-RR method to circuit problems in which the system matrices in multiple regions need to be reduced separately. Numerical and experimental results are given to demonstrate its validity.* © 2008 Wiley Periodicals, Inc. Microwave Opt Technol Lett 50: 2337–2341, 2008; Published online in Wiley InterScience (www.interscience.wiley.com). DOI 10.1002/mop.23630

Key words: *time-domain; finite element method; electromagnetic analysis; high frequency; integrated circuits*

1. INTRODUCTION

In the past three decades, driven by the continuous scaling of feature sizes and frequency, on-chip circuits have witnessed a series of transitions in modeling technology: from R (resistance)-based, RC (resistance-capacitance)-based, distributed RC-based, and RLC (resistance-inductance-capacitance)-based to transmission-line-based to full-wave electromagnetics-based analysis [1–8]. The increased level of integration across the entire electromagnetic spectrum necessitates the electromagnetics-based analysis even more. However, on-chip circuits present many modeling challenges [6] that are less pronounced in traditional full-wave applications such as antennas and waveguides. Among them, problem size is the No. 1 challenge. Ultra large-scale integration results in numerical problems of ultra large scale, requiring billions and billions of parameters to describe them accurately. In [7], to overcome the large problem size, a time-domain layered finite element reduction recovery (LAFE-RR) method was developed for high-frequency modeling and simulation of large-scale on-chip circuits. This method rigorously reduces the matrix of a multilayer system to that of a single-layer system, regardless of the original problem size. More importantly, the matrix reduction is achieved analytically, and hence the CPU and memory overheads are minimal. In addition, the reduction preserves the sparsity of the original system matrix. Numerical experiments have demonstrated four-orders-of-magnitude reduction in matrix factorization time. The superior performance applies to any arbitrarily shaped multilayer structure.

In this article, an alternative analytical reduction algorithm is proposed to further improve the capability of the LAFE-RR method. With this algorithm, the LAFE-RR method is generalized to support a variety of absorbing boundary conditions which cannot be supported by the original analytical reduction algorithm. In addition, it permits the application of the LAFE-RR method to circuit problems in which system reduction needs to be done separately for different regions.

2. FORMULATION

For the practical use of the LAFE-RR method, absorbing boundary conditions (ABCs) often need to be incorporated to truncate the computational domain. For example, in Figure 1, a circuit region of L layers is attached to two ABC regions, in which the outgoing waves are absorbed. The ABC region can be filled with air backed by a first-order absorbing boundary condition, or can be filled with

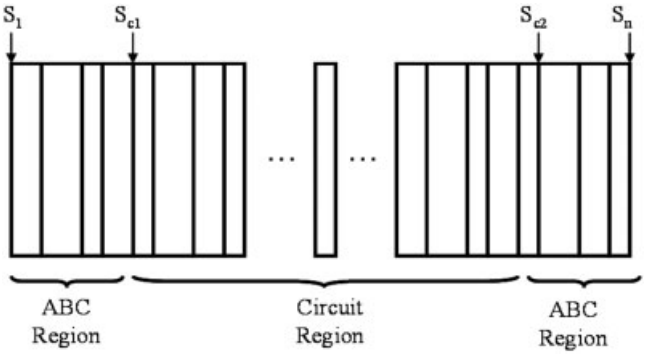

Figure 1 A circuit region attached to two ABC regions

perfectly matched layers (PMLs) for better absorption when the radiation from the structure is strong. The configuration of the permittivity and conductivity in the ABC region can be very different from that in the circuit region. This could invalidate the interlayer linear proportionality between the off-diagonal and diagonal matrices when combining the circuit region with the ABC region, and hence rendering the analytical reduction in the LAFE-RR method not feasible. However, the linear proportionality between the off-diagonal and diagonal matrices still holds true in the circuit region itself and in the ABC region itself. In this case, an alternative reduction scheme is needed, which, instead of reducing the system matrix to that of layer l ($l = 1, 2, \ldots, L$), reduces the system matrix to a matrix that is formed by the unknowns residing on the boundaries of each region so that the reduced matrix can interface with the system matrix in other regions easily. Take the circuit region shown in Figure 1 as an example. The system matrix of the circuit region is reduced to a matrix that is formed by unknowns residing on S_{c1} and S_{c2}.

The aforementioned alternative reduction scheme is not only needed for the use of general ABCs, but also needed when the computational domain encompasses multiple circuit regions, each of which features a different semiconductor process such that a single analytical LAFE-RR treatment across the entire domain is not feasible.

In Figure 2, the basic procedure of the alternative reduction scheme is illustrated. The submatrix in layer l ($l = 1, 2, \ldots, L$) is denoted by $\mathbf{P}_{sl}$, which is made of $\mathbf{M}_l$ and $\mathbf{K}_l$ $\mathbf{M}_l$ and $\mathbf{K}_l$ are assembled from their elemental contributions as:

$$\mathbf{M}^e_{l,ij} = \frac{h_l}{3}(\mu_0\varepsilon^e_l)\iint_{\Omega^e} \mathbf{W}_i \cdot \mathbf{W}_j d\Omega$$

$$\mathbf{K}^e_{l,ij} = \frac{h_l}{6}(\mu_0\varepsilon^e_l)\iint_{\Omega^e} \mathbf{W}_i \cdot \mathbf{W}_j d\Omega l = 1,2,\cdots L \tag{1}$$

in which subscript l is the layer index, Ω^e denotes each triangular element, $\mathbf{W}_i$ is the well-known edge vector basis function, h_l is the thickness of layer l, and ε^e_l is the permittivity of layer l in element e.

To obtain a reduced system matrix that only involves the unknowns residing on the first surface (surface 1) and the last surface (surface L), first, we "add" $\mathbf{P}_{s1}$ with $\mathbf{P}_{s2.}$ The "addition" here is not a normal addition. Instead, it is a superposition of submatrices at the interface between layer 1 and layer 2. We then eliminate the interface unknowns, and obtain matrix $\mathbf{P}_{s,12}$ that is made of $\mathbf{A}_2$, $\mathbf{B}_2$, and $\mathbf{C}_2$ as shown in Figure 2. We then add $\mathbf{P}_{s,12}$ with $\mathbf{P}_{s,3}$. Again, the addition here is a superposition at the interface. By eliminating the interface unknowns, we obtain $\mathbf{P}_{s,13}$ that is made of $\mathbf{A}_3$, $\mathbf{B}_3$, and $\mathbf{C}_3$. We then add $\mathbf{P}_{s,13}$ with $\mathbf{P}_{s,4.}$ We continue this procedure until we obtain $\mathbf{P}_{s,1L}$ which only involves the unknowns on the first surface and the last surface. This procedure can be applied to any region to reduce the multilayered system matrix to a single-layer one that only involves surface unknowns residing on the two boundaries of the region.

The procedure shown in Figure 2 can be mathematically represented by

$$\begin{aligned}
&\mathbf{A}_1 = \mathbf{M}_1, \quad \mathbf{B}_1 = \mathbf{K}_1, \quad \mathbf{C}_1 = \mathbf{A}_1\\
&\mathbf{A}_l = \mathbf{A}_{l-1} - \mathbf{B}_{l-1}(\mathbf{C}_{l-1} + \mathbf{M}_l)^{-1}\mathbf{B}^T_{l-1}\\
&\mathbf{B}_l = -\mathbf{B}_{l-1}(\mathbf{C}_{l-1} + \mathbf{M}_l)^{-1}\mathbf{K}_l\\
&\mathbf{C}_l = \mathbf{M}_l - \mathbf{K}_l(\mathbf{C}_{l-1} + \mathbf{M}_l)^{-1}\mathbf{K}_l, \; l = 2,3,\ldots,L.
\end{aligned} \tag{2}$$

In a multilayered structure, as shown by (1), M_l and $\mathbf{K}_l$ are linearly proportional to each other in the same layer as well as in different layers. Hence there is no need to evaluate matrix inverse and matrix–matrix multiplication in (2). The matrix operation in (2) becomes a scalar operation. To elaborate, we denote the final reduced matrix $\mathbf{P}_{s,1L}$ shown in Figure 2 by

$$\mathbf{A}_L = a_L\mathbf{U}, \quad \mathbf{B}_L = b_L\mathbf{U}, \quad \mathbf{C}_L = c_L\mathbf{U} \tag{3}$$

in which U is common to every layer, and a_L, b_L, and c_L are coefficients to be determined. If the layer-growth direction is chosen as z (stack-growth direction), $\mathbf{U}$ is

$$\mathbf{U} = \frac{1}{3}(\mu_0)\iint_{\Omega} \mathbf{W}_i \cdot \mathbf{W}_j d\Omega. \tag{4}$$

If the layer-growth direction is chosen from x or y, U is assembled from

$$\mathbf{U}^e = \frac{1}{3}(\mu_0\varepsilon^e)\iint_{\Omega^e} \mathbf{W}_i \cdot \mathbf{W}_j d\Omega. \tag{5}$$

The coefficients a_L, b_L, and c_L in (3) can be obtained from the following recursive procedure as a direct consequence of (2)

$$\begin{aligned}
&a_1 = \varepsilon_1 h_1, \quad b_1 = 0.5\varepsilon_1 h_1, \quad c_1 = a_1\\
&a_l = a_{l-1} - b_{l-1}(c_{l-1} + \varepsilon_l h_l)^{-1}b_{-1}\\
&b_l = -b_{l-1}(c_{l-1} + \varepsilon_l h_l)^{-1}0.5\varepsilon_l h_l
\end{aligned}$$

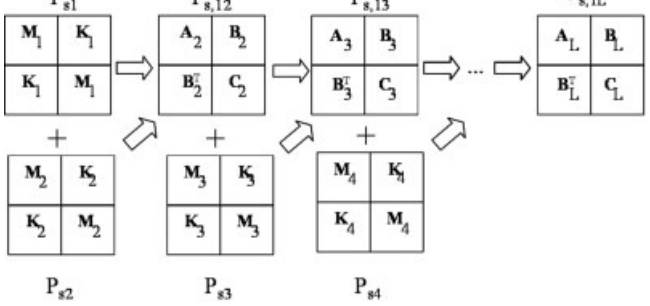

Figure 2 An alternative reduction scheme

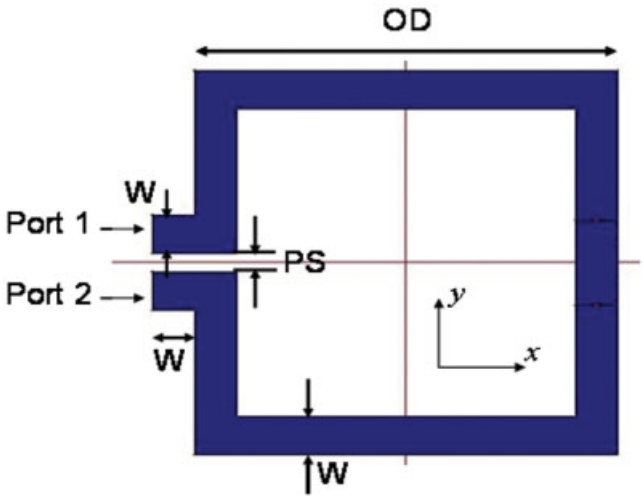

Figure 3 Geometry of a symmetric square inductor (OD = 1000 mm, W = 100 mm, PS = 50 mm). [Color figure can be viewed in the online issue, which is available at www.interscience.wiley.com]

$$c_l = \varepsilon_l h_l - 0.5\varepsilon_l h_l (c_{l-1} + \varepsilon_l h_l)^{-1} 0.5\varepsilon_l h_l,\ l = 2,3,\ldots,L \tag{6}$$

in which ε_l ($l = 1, 2, \ldots, L$) is the relative permittivity of layer l if the layer-growth direction is chosen as z, and 1 otherwise.

The right-hand side of the system matrix equation also needs to be updated. The updating scheme can be mathematically expressed as

$$b'_{S_1} = b_{S_1}, \quad b'_{S_L+1} = b_{S_2}$$

$$b'_{S_1} = b'_{S_1} - \mathbf{B}_{l-1}(\mathbf{C}_{l-1} + \mathbf{M}_l)^{-1} b'_{S_L+1}$$

$$b'_{S_L+1} = b_{S_L+1} - \mathbf{K}_l(\mathbf{C}_{-1} + \mathbf{M}_l)^{-1} b'_{S_L+1},\ l = 2,3,\ldots,L. \tag{7}$$

in which b_{S_1} ($l = 1, 2, \ldots, L$) is the right hand side corresponding to the unknowns on S_i in the original system matrix, b'_{S_1} and b'_{S_L+1} are the updated right hand side in the reduced system matrix, which correspond to unknowns residing on S_1, and S_{L+1} respectively. Because of the linear proportionality between $\mathbf{M}_l$ and $\mathbf{K}_l$, again there is no need to evaluate matrix inverse and matrix-vector multiplication in (7). Vectors b'_{S_1} and b'_{S_1} can be obtained recursively from

$$b'_{S_1} = b_{S_1}, \quad b'_{S_L+1} = b_{S_2}$$

$$\text{do from } l = 2 \text{ to L}$$

$$b'_{S_1} = b'_{S_1} - b_{l-1}(c_{l-1} + \varepsilon_l h_l)^{-1} b'_{S_L+1}$$

$$b'_{S_L+1} = b_{S_L+1} - 0.5\varepsilon_l h_l (c_{l-1} + \varepsilon_l h_l)^{-1} b'_{S_L+1}$$

$$\text{end do} \tag{8}$$

With the aforementioned alternative reduction scheme, the reduced system matrix equation becomes:

$$\begin{pmatrix} \mathbf{A}_L & \mathbf{B}_L \\ \mathbf{B}_L & \mathbf{C}_L \end{pmatrix} \begin{Bmatrix} x_{S_1} \\ x_{S_L+1} \end{Bmatrix} = \begin{Bmatrix} b'_{S_1} \\ b'_{S_L+1} \end{Bmatrix} \tag{9}$$

which involves unknowns on the first and last surfaces only. This matrix equation can be conveniently stitched with the matrix equations in other regions to perform the simulation in the entire computational domain.

3. NUMERICAL RESULTS

To validate the proposed alternative reduction scheme, we simulated a symmetric square inductor. This example was characterized by the frequency-domain layered finite element method in [8]. However, it cannot be simulated by the time-domain LAFE-RR method proposed in [7] because the analytical reduction scheme developed in [7] cannot be applied across the circuit region and the ABC region that is filled by a different material. For all the examples simulated in [7], either an exact absorbing boundary condition is used or the dielectric stack is extended and then truncated directly by a first-order absorbing boundary condition.

The geometrical dimensions of the inductor are shown in Figure 3. The inductor is designed on a metal layer of thickness 15 μm. It is backed by a ground plane that is 15 μm thick. There is an interlayer dielectric medium of relative permittivity 3.4 and thickness 30 μm between the inductor metal layer and the ground plane. There exists a perfect electrically conducting (PEC) plane at the top, which is separated from the inductor metal layer by an interlayer dielectric medium of relative permittivity 3.4 and thickness 650 μm. The relative permittivity of the inductor layer is 3.4. All metals have conductivity 5.8×10^7 S/m.

The ABC region is attached to the inductor structure from the left, right, front (port side), and back. No ABC region is needed at the bottom and at the top because the inductor is backed by a PEC boundary therein. The thickness of the ABC region is 50 μm in the front and at the back, and 100 μm at the left and right. The ABC region is an air region that is backed by a first-order absorbing boundary condition. The air region is used to facilitate the extraction of open circuit voltage which is needed in our S-parameter extraction flow [8]. The layer-growth direction is chosen as x (refer to Figure 3 for direction), along which, the computational domain is discretized into 24 layers, rendering 57514 unknowns. The alternative reduction scheme proposed in this article is used to reduce the 22 layers in the

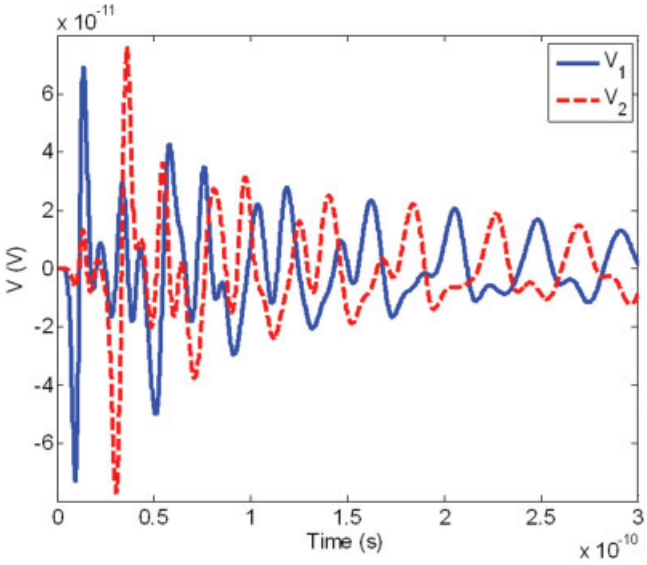

Figure 4 Time-domain voltages sampled at two ports. [Color figure can be viewed in the online issue, which is available at www.interscience.wiley.com]

middle to a single-layer matrix that interfaces with the two matrices of the ABC regions in the front and at the back. A current probe is vertically attached from the ground plane to the two inductor ports in turn. Voltages are sampled at the two ports from which the S-parameters are extracted. The current source is a derivative of Gaussian pulse, $2(t - t_0)\exp(-(t - t_0)^2/\tau^2)$, in which τ is 7e-11, and t_0 is 4τ. Figure 4 depicts the voltage waveforms sampled at port 1 and port 2 respectively when port 1 is excited. The resonance of an LC-type circuit can be clearly seen. The S-parameters are then extracted from the time-domain responses. As shown in Figure 5, they agree very well with the data generated by a commercial full-wave tool, HFSS, which validates the proposed new reduction scheme.

With the new scheme validated, we have applied it to simulate large-scale on-chip structures. Shown in Figure 6 is the crosstalk of a large-scale test-chip interconnect structure. Because of a nondisclosure agreement, the detail of this structure is not given here. The finite-element discretization results in a 7,255,818-unknown system, which cannot be factorized by a traditional time-domain finite-element method on a computer with 1 GB memory. In contrast, the proposed method analytically, i.e., without any computational cost, reduces the original large-scale system to a sparse matrix of size 7272, which is factorized within a few seconds. The crosstalk is extracted at the near ends of two interconnect wires residing in metal 2 layer. As shown by Figure 6, the simulated crosstalk agrees well with the measured data in both magnitude and phase.

4. CONCLUSION

In this article, an alternative analytical reduction scheme is proposed for the time-domain LAFE-RR analysis of high-frequency VLSI circuits. This scheme permits the use of general ABCs in the framework of the LAFE-RR method. It also permits the application of the analytical reduction scheme in the LAFE-RR method to circuit problems that require different reductions in different regions. Numerical and experimental results demonstrate its validity.

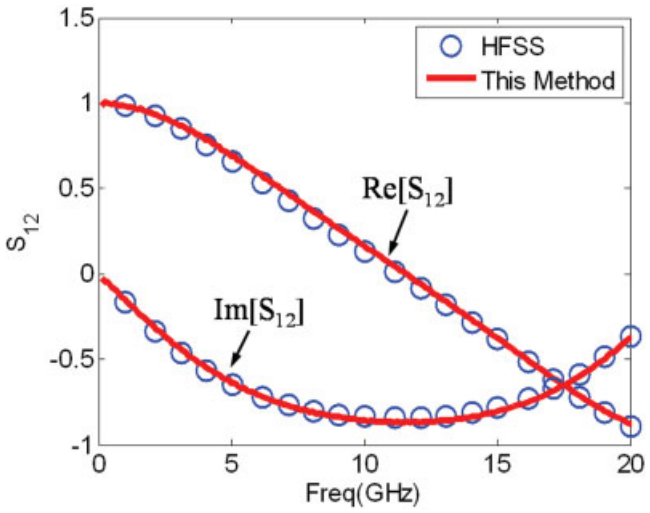

Figure 5 Simulated crosstalk in comparison with HFSS results. [Color figure can be viewed in the online issue, which is available at www.interscience.wiley.com]

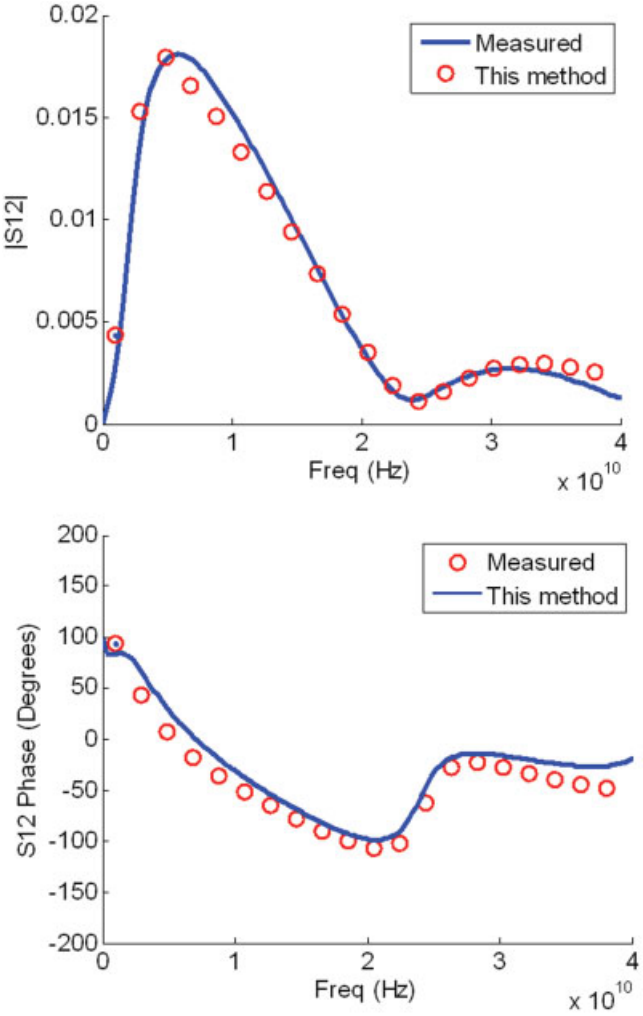

Figure 6 Simulation of a large-scale test-chip interconnect. (a) Magnitude of the crosstalk. (b) Phase of the crosstalk. [Color figure can be viewed in the online issue, which is available at www.interscience.wiley.com]

ACKNOWLEDGMENTS

The authors would like to thank M. J. Kobrinsky at Intel Corporation for providing measured data. This work was supported by a grant from Office of Naval Research under award N00014-06-1-0716.

REFERENCES

1. P.J. Restle, A.E. Ruehli, S.G. Walker, and G. Papadopoulos, Full-wave PEEC time-domain method for the modeling of on-chip interconnects, IEEE Trans CAD 20 (2001), 877–887.
2. A. Rong, A.C. Cangellaris, and L. Dong, Comprehensive broadband electromagnetic modeling of on-chip interconnects with a surface discretization-based generalized PEEC model, IEEE 12th Topical Meeting on Electrical Performance of Electronic Packaging (2003), 367–370.
3. Z.H. Zhu, B. Song, and J.K. White, Algorithms in FastImp: A fast and wideband impedance extraction program for complicated 3D geometries, IEEE Trans CAD 24 (2005), 981–998.
4. D. Gope, A.E. Ruehli, C. Yang, and V. Jandhyala, (S)PEEC: Time- and frequency-domain surface formulation for modeling conductors and dielectrics in combined circuit electromagnetic simulations, IEEE Trans MTT 54 (2006), 2453–2464.
5. Z.G. Qian, J. Xiong, L. Sun, I.T. Chiang, W.C. Chew, L.J. Jiang, and Y.H. Chu, Crosstalk analysis by fast computational algorithms, IEEE

14th Topical Meeting on Electrical Performance of Electronic Packaging (2005), 367–370.
6. D. Jiao, C. Dai, S.-W. Lee, T.R Arabi, and G. Taylor, Computational electromagnetics for high-frequency IC design, IEEE International Symposium on Antennas and Propagation (2004), 3317–3320.
7. H. Gan and D. Jiao, A time-domain layered finite element reduction recovery (LAFE-RR) method for high-frequency VLSI design, IEEE Trans Antenna Propag 55 (2007), 3620–3629.
8. D. Jiao, S. Chakravarty, and C. Dai, A layered finite element method for electromagnetic analysis of large-scale high-frequency integrated circuits, IEEE Trans Antenna Propag 55 (2007), 422–431.

EXPERIMENTAL DEMONSTRATION OF NARROW BEAM MONOPOLE ANTENNA EMBEDDED IN LOW EFFECTIVE INDEX OF REFRACTION ($n < 1$) WIRE MEDIUM

Rongguo Zhou,[1] Hualiang Zhang,[2] and Hao Xin[1,2]
[1] Department of Physics, University of Arizona, Tucson, AZ 85721; Corresponding author: hxin@ece.arizona.edu
[2] Department of Electrical and Computer Engineering, University of Arizona, Tucson, AZ 85721

Received 3 January 2008

ABSTRACT: *A narrow beam monopole antenna is realized by embedding the antenna within a periodic metallic wire array. The 2D wire array is designed to have an effective index of refraction smaller than unity ($n_{eff} < 1$) at the X-band frequencies (8–12 GHz), within which the antenna operates. The narrow beam effect due to the low refractive index of the wire medium is demonstrated in both simulation and experiment. Measured antenna properties including return loss and radiation pattern are in good agreement with simulation results. This simple and straightforward antenna design methodology can be applied at any microwave frequency.* © 2008 Wiley Periodicals, Inc. Microwave Opt Technol Lett 50: 2341–2345, 2008; Published online in Wiley InterScience (www.interscience.wiley.com). DOI 10.1002/mop.23653

Key words: *metallic wire array; metamaterial; narrow beam antenna*

1. INTRODUCTION

Recently, various investigations have been reported on metamaterials with near-zero permittivity (ε) and/or index of refraction (n) because of their useful applications such as, highly directive beams [1], compact resonators [2], zero phase delay lines [3], wave front transformers [4], transparent coating [5], and subwavelength tunneling [6]. As a simple metamaterial with frequency dependent permittivity ε, periodic metallic wire structures have been analyzed by applying plasma theory [7] and used to achieve narrow beam antennas [1, 8–10]. In Refs. 1, 8, and 9, the structures used to achieve directive radiation were based on a ground-plane backed metamaterial slab composed of rows of metallic wires with finite length, for which the effective medium parameters could not be directly estimated by the simple plasma theory. And most of the previous work did not apply effective medium parameters of the wire array in the antenna designs [1, 9, 10].

In this article, an effectively infinite long metallic wire array, which is realized by terminating the wires with conducting plates, is designed to have an effective index of refraction less than unity at X-band (8–12 GHz). The design is confirmed by the extracted effective medium parameters from finite-element simulation results. A simple design methodology for narrow beam antenna is then introduced by embedding a monopole antenna in this low refractive index metallic wire medium. As illustrated in Figure 1, when a source is placed in a medium with $n_2 < 1$, at the boundary between this medium and free space, Snell's law ($n_1 \sin\theta_1 = n_2 \sin\theta_2$, $n_1 = 1$, with the assumption of plane waves) requires that the refractive angle θ_1 is less than θ_2, indicating that the electromagnetic wave will be refracted toward the normal direction of the interface and a radiation beam narrowing effect can be achieved. To demonstrate this effect, an experimental prototype is fabricated and measured. The measured radiation patterns show symmetrical narrowed beams in 4-directions. We also apply three metal reflectors around the wire arrays to achieve a single-beam antenna with directional radiation. Both simulation and experimental results regarding these metallic wire array enabled antenna systems are reported here.

2. DESIGN OF THE METALLIC WIRE ARRAY

The proposed 2D wire array structure is shown in Figure 2. This structure is composed of an infinite number of periodic metallic wires in the x and y directions with infinite length in the z direction. The wire radius is 0.25 mm and the spacing between adjacent wires is 9 mm in both x and y directions. The effective permittivity of this kind of wire arrays was derived using plasma theory as a function of the wire array periodicity a, the wire radius r, and frequency ω (under the assumption that $r << a$) [7]:

$$\varepsilon_{\text{eff}} = 1 - \omega_p^2/\omega^2 = 1 - 2\pi c^2/[a^2 \ln(a/r)\omega^2], \quad (1)$$

where c is the speed of light and ω_p is the plasma frequency at which the effective permittivity ε_{eff}, and thus the effective index of refraction n_{eff}, is zero.

According to Eq. (1), the plasma frequency of the proposed wire array is $f_p = \omega_p/(2\pi) = 7.02$ GHz. Because of the finite radius of the wires, finite element simulation is necessary to extract the exact effective medium properties of the wire array. Ansoft high frequency structure simulator (HFSS) is used to simulate the scattering parameters (or the transmission and reflection coefficients) of the wire array structure. In the HFSS model, the incident plane wave is polarized along the wires and four unit cells are

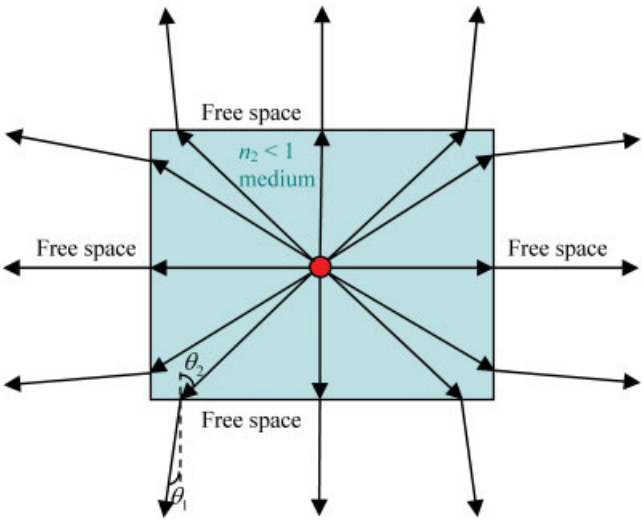

Figure 1 Geometrical illustration of directive beam in $n < 1$ medium. [Color figure can be viewed in the online issue, which is available at www.interscience.wiley.com]